ACS APPLIED MATERIALS & INTERFACES

Research Article

www.acsami.org

Ultrathin and Lightweight 3D Free-Standing Ni@NiO Nanowire Membrane Electrode for a Supercapacitor with Excellent Capacitance Retention at High Rates

Nishuang Liu,*[,†] Jian Li,[†] Wenzhen Ma,[†] Weijie Liu,[†] Yuling Shi,[†] Jiayou Tao,[†] Xianghui Zhang,[†] Jun Su,[†] Luying Li,[†] and Yihua Gao*[,†,‡]

[†]Center for Nanoscale Characterization & Devices (CNCD), Wuhan National Laboratory for Optoelectronics (WNLO)-School of Physics, Huazhong University of Science and Technology (HUST), 1037 Luoyu Road, Wuhan 430074, China

[‡]Hubei Collaborative Innovation Center for Advanced Organic Chemical Materials, 368 Youyi Avenue, Wuhan 430062, China

Supporting Information

ABSTRACT: A free-standing binder-free 3D Ni@NiO nanowire membrane is fabricated by a simple filtration method followed by thermal annealing. With an appropriate annealing temperature, the functional nanowires can keep their rough and echinate surface, and the conductive network composed of welded nickel nanowire cores is well-preserved without isolation (0.53 Ω/sq). The unique 3D multigrade mesporous structure not only accelerates the intercalation and deintercalation velocity of electrolyte ions but also provides numerous electroactive sites for the Faraday reaction. As a result, the supercapacitor electrode can preserve a capacitance retention of 96.1% (36.9 F/cm^3) with a high discharge current density, indicating its wonderful rate capability. The fabricated membrane electrode exhibits high volumetric capacitance, stable cycling life, and remarkable retention of the capacitance at high rate, energy, and power density, making it a promising candidate for application in portable electronic products.

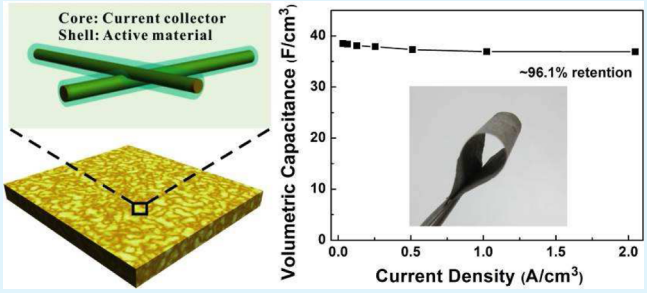

KEYWORDS: *supercapacitors, free-standing, binder-free, Ni@NiO nanowire, high rate capability*

INTRODUCTION

Owing to the promising features of fast charge/discharge rate, high power delivery, and long cycling lifespan, a supercapacitor can be a very fascinating alternative to batteries by balancing the need of the high power density of a capacitor and the high energy density of a battery[1−4] and already has attracted great interest in the field of energy conversion/storage and power output technology, such as portable consumer electronic products, hybrid electric vehicles, etc.[5−8] Usually, according to the underlying charge-storage mechanism, supercapacitors can be divided into two groups: electrochemical double-layer capacitors (EDLCs) and pseudocapacitors. The capacitance of EDLCs solely comes from the charge separation arising at the interface between the electrode and electrolyte,[9] which generally leads to limited specific capacitance.[10,11] However, because of the fast and reversible multielectron redox Faradaic reactions of redox-active materials, pseudocapacitors with active materials of transition-metal oxides such as MnO_2, nickel oxide (NiO), and Co_3O_4 may achieve much higher specific capacitances.[12−16] Unfortunately, the poor electrical and ionic conductivity of these active materials of transition-metal oxides usually depresses their capacitor performance, especially at high rates.[17,18] Traditional slurry-coating technology is the most commonly used method to fabricate electrodes for supercapacitors, in which active materials are mixed with binder and conductive additives on a current collector.[19,20] As a consequence, the binder not only blocks a large part of the direct contact among electroactive surfaces of active materials and electrolyte but also decreases the electrical conductivity of the electrode, both suppressing the capacitor performance.[21]

Most recently, the assembly of 1D nanowires (or nanotubes) and 2D nanosheets into 3D macroscopic membranes has been studied intensively because these 3D free-standing membranes hold many novel intrinsic characteristics, including high porosity, large specific surface area, and good flexibility.[21−27] Especially, this kind of method offers a great opportunity to fabricate a high-performance flexible binder-free supercapacitor electrode, in which all of the materials could take part in the charge-storage process with their surface in direct contact with the electrolyte.[10,21,28−32] Furthermore, when the overall volume of the device is considered, this design of an electrode can significantly improve the total performance and shows promising potential to enhance the volumetric capacitance for a supercapacitor. Generally, free-standing and binder-free electrodes are prepared by a simple filtration method, by which pseudocapacitor-active materials with poor electrical

Received: May 20, 2014
Accepted: July 30, 2014
Published: July 30, 2014

conductivity are usually mixed homogeneously with carbon nanotubes (CNTs) or graphene, which act as conductive additives besides EDLC materials, followed by filtration to yield paperlike electrodes.[10,21,28−32] For these binder-free electrodes, a 3D conductive network composed of CNTs or graphene can play the roles of an embedded current collector and mechanical supporting frame.[10,21,28−32] However, there are still some challenges, such as poor electrical conductivity of active materials blocking the contact between conductive CNTs (or graphene), limited electrical contact area, and weakly physical contact without any strong interfacial interactions among active materials and CNT (or graphene) conductive networks, which leads to poor electron transport through active materials to a conductive network and great reduction of their capacitor performance at high rates as a result.[27] To solve this challenge, it must be highly necessary to improve the interfacial interactions among active materials and a conductive network for a binder-free supercapacitor electrode with high rate capability.

In this work, as a proof-of-concept experiment, we develop an effective method to fabricate a free-standing binder-free Ni@NiO membrane supercapacitor electrode, via a simple filtration method followed by thermal annealing. We chose nickel (Ni) as the original material because of its high conductivity, its high oxidation resistivity,[33] and the excellent pseudocapacitor performance of its oxide, NiO, as an active material of low cost, environment friendliness, and high theoretical specific capacitance (2584 F/g),[34] which is a promising potential electrode material for a supercapacitor. In order to prepare ultralong Ni nanowire, which is necessary for a free-standing binder-free electrode, a simple liquid-phase method with the help of a magnetic field has been applied, using the ferromagnetic properties of Ni nanoparticles. After vacuum filtration, a pressing process, and preannealing in H_2/Ar, entangled and well-welded Ni nanowires can form a free-standing binder-free membrane with high conductivity and good mechanical properties. Via simple annealing in the open air, active materials of NiO can be achieved on the surfaces of Ni nanowires with strong interfacial interactions and robust linking to the embedded Ni nanowire conductive network, which would enable a good electrical contact and be useful to form a fast channel to transfer the interface electrons between NiO and Ni. In this unique structured electrode, the "core" Ni nanowire conductive network acts as a highly efficient current collector, while the "shell" NiO layers play the role of active materials. Most importantly, unlike other binder-free electrodes, direct electrical contact between conductive Ni nanowires can be guaranteed because every Ni nanowire is well-welded to each other despite the poor conductive NiO layer on their surfaces, as shown in the schematic illustration of Figure 1a. Benefiting from this design, we believe the familiar problems in binder-free electrodes such as blocked contact between conductive networks, restricted electrical contact area, and weak contact among active materials and a current collector can all be resolved at once. Accordingly, an excellent capacitor performance at high rates can be predicted for this free-standing binder-free supercapacitor electrode.

RESULTS AND DISCUSSION

As shown in the digital photograph of Figure 1b, a uniform free-standing Ni nanowire membrane can be obtained by section filtration of the precipitate and heat treatment. Its X-ray diffraction (XRD) pattern is presented by Figure 1c. The

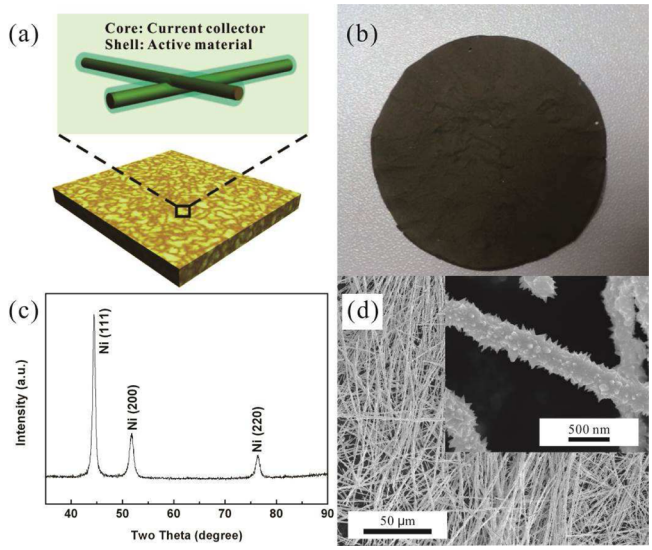

Figure 1. (a) Schematic illustration of the 3D free-standing binder-free Ni@NiO nanowire membrane. The "core" Ni nanowire networks and "shell" NiO layer work as a current collector and active materials, respectively. (b) Optical image of the Ni nanowire membrane. (c) XRD spectra of the Ni nanowire product. (d) SEM images of the Ni nanowire products.

pattern of the product matches well with a Ni face-centered-cubic structure (JCPDS no. 04-0850). The peaks at (2θ) 44.62°, 51.94°, and 76.58° correspond to (111), (200), and (220) of crystalline Ni, respectively. There are no other characteristic peaks, which indicates that pure Ni nanowires have been obtained. Scanning electron microscopy (SEM) images of Figure 1d reveal the microstructure of the ultralong Ni nanowire. From it, we can see that ultralong Ni nanowires with a length of more than 200 μm and a diameter of about 350 nm can be obtained via this simple liquid-phase method. Furthermore, as illustrated in the SEM images, the Ni nanowires were constituted of a lot of embossment, in morphology uneven in a small region but uniform on the whole. The rough surface can effectively increase their specific surface areas, which also enhances the potential for the electrochemical performance. To characterize the electrical property of the 3D Ni nanowire membrane, a standard four-point-probe method was taken. A sheet resistance as low as 0.21 Ω/sq was calculated for the membrane, revealing its wonderful electrical conductivity. Generally, Ni foam is widely used in supercapacitors[35] as current collectors because of their open pore structure, high specific surface area, and good electrical conductivity. However, Ni foam has a pore size of about 250 μm, which is too large. So much space is unprofitable and volumetrically wasteful (as shown in Figure S2 in the Supporting Information, SI). Compared with the commercial Ni foam, the Ni nanomembrane consists of Ni nanowires with nanoscale pores rather than hundreds of micron scale. To probe the porous structure of the membrane, nitrogen adsorption/desorption isotherms are measured. The specific Brunauer−Emmett−Teller surface area is about 0.81 m^2/g, which is much higher than the value of commercial Ni foam.[36] The Barrett−Joyner−Halenda adsorption average pore diameter and desorption average pore diameter are about 46.9 and 38.8 nm. Therefore, the nanomembrane has a much higher specific surface area, a more reasonable hole size, and a very thin thickness of less than 26 μm. On the basis of these facts,

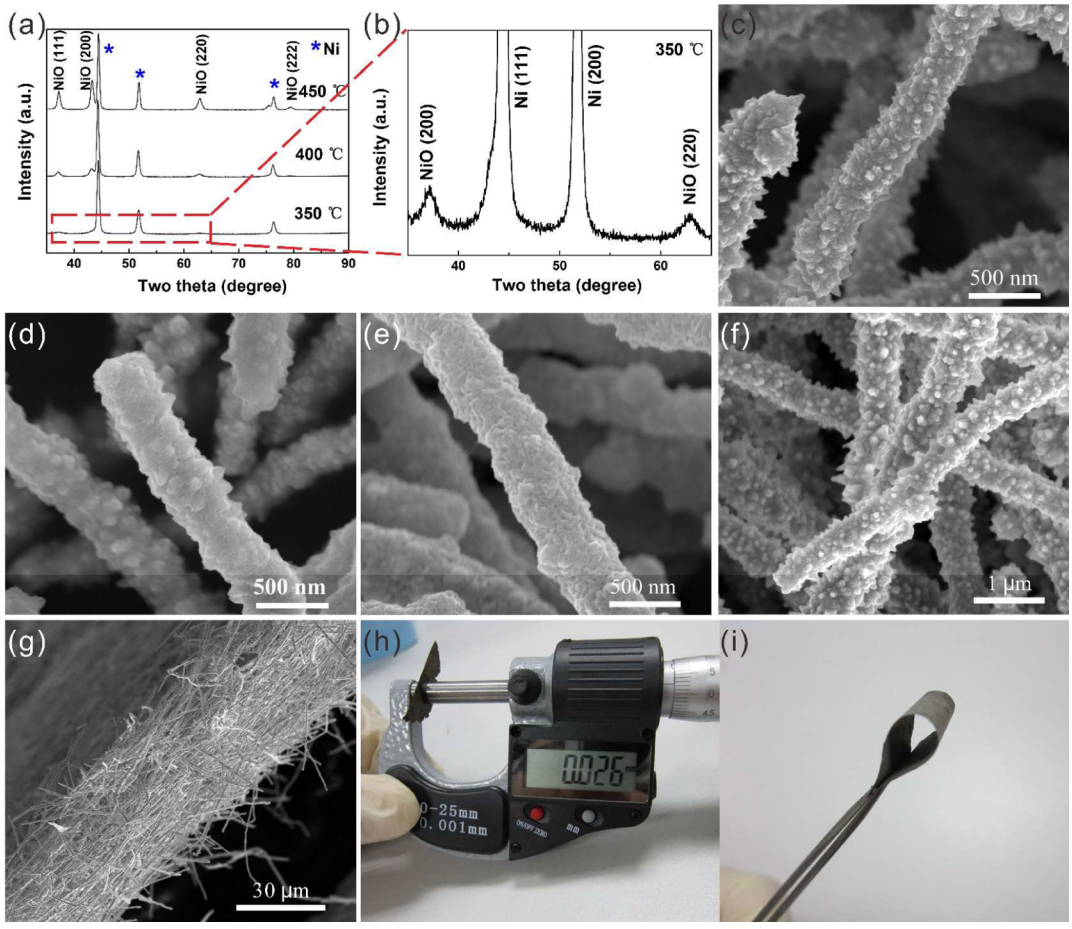

Figure 2. (a and b) XRD spectra of products calcined at different temperatures in the open air. SEM images of Ni@NiO nanowires calcined at (c) 350, (d) 400, and (e) 450 °C, respectively. (f) SEM image of a large number of Ni@NiO nanowires welded and linked together with their cross sections embedded in each other. (g) Cross-sectional SEM image of the ultrathin 3D mesporous free-standing Ni@NiO nanowire membrane. (h) Macroscopic test via a spiral micrometer to measure the thickness of the free-standing Ni@NiO membrane (26 μm). (i) Digital image of the free-standing binder-free Ni@NiO membrane annealed at 350 °C, possessing high flexibility without any obvious mechanical damage even under severe bending conditions.

we believe the 3D free-standing Ni nanomembrane has the potential to be a very attractive alternative to the Ni foam.

To achieve the active material of NiO, the free-standing Ni nanowire membrane was annealed in a muffle furnace. In order to choose an appropriate temperature, thermogravimetric analysis (TGA) was performed for the membrane in the open air on a thermal analyzer. According to the curve shown in Figure S3 in the SI, we can observe that the significant weight increment of the precursors occurred from about 300 to 600 °C, suggesting that the Ni nanowire precursors oxidized completely to become NiO above approximately 600 °C. Considering that only a small amount of NiO is needed as active material, three temperatures of 350, 400, and 450 °C were taken as the annealing temperature. Additionally, parts a and b of Figure 2 presents XRD patterns of a Ni@NiO free-standing membrane calcined for 5 min at those three different temperatures in the open air. The patterns not only had the peaks contributed from the Ni at the same diffraction angle but also contained some new diffraction peaks. These peaks match well with the NiO face-centered-cubic structure (JCPDS no. 73-1519). The diffraction angles of 37.34° and 63.02° were attributed to (111) and (200) of NiO, respectively. As the calcination temperature rises, the number of NiO peaks increased from two (350 °C, in Figure 2a) to three (400 °C) and four (450 °C). Also, the diffraction intensity increased as well. All of these data identified that the ratio of NiO increased, and the crystallinity was improved. The morphology and diameter of Ni@NiO nanowires also changed greatly with increasing calcination temperature, as shown in the SEM images of Figure 2c–e. The surfaces of the nanowires were rather rough and echinate (350 °C) and became smooth with higher annealing temperature. Also, the diameter increases from about 350 to 500 nm.

We also measured the electrical property of the annealed membranes via a four-point-probe method, and the values of sheet resistance were 0.53, 3.4, and 8.6 Ω/sq for the samples of 350, 400, and 450 °C, respectively, which means oxidization on the surface layer of the Ni nanowire network only slightly reduces the conductivity of the Ni@NiO nanowire membrane. In order to find microscopic evidence for this result, more detailed characterization has been performed on the sample. As shown in the SEM image of Figure 2f, many Ni@NiO nanowires are welded and linked together with their cross sections embedded in each other and integrated into a network (in Figure S4a in the SI), which is consistent with the schematic illustration in Figure 1a. Figure 2g shows the cross-sectional SEM image of the ultrathin free-standing Ni@NiO membrane, revealing the uniform mesporous film with a thickness of less

dx.doi.org/10.1021/am503108x | ACS Appl. Mater. Interfaces 2014, 6, 13627–13634

than 30 μm, while macroscopic measurement via a spiral micrometer further confirms this result with a value of 26 μm. Additionally, Figure S4b in the SI is the enlarged cross-sectional image, indicating that the Ni@NiO nanowires are well-welded and linked together and the nanowires are distributed uniformly in the network to form a free-standing membrane with a large number of nanoscale pores. The interconnected Ni@NiO nanowire networks not only ensure the mechanical strength of the free-standing membrane but also offer many critical advantages for application in a supercapacitor. First, the Ni@NiO nanowire membrane possesses a large number of hierarchical porous channels, which can actually accelerate the intercalation and deintercalation velocity of electrolyte ions into the 3D nanostructured electrode.[37,38] Second, the highly conductive Ni nanowires are welded and embedded in each other and form a conductive network as a current collector, despite the NiO layer on the surface with poor conductivity, enabling efficient current collection and unobstructed electron transport. Third, the mesoporous structures of the Ni@NiO network and the nanoscale thorns on the surface of the ultralong nanowires both provide high surface areas, which lead to efficient utilization of the active NiO. On the basis of those advantages mentioned above, we believe the 3D Ni@NiO membrane would be an ideal binder-free supercapacitor electrode. The membrane was weighted to be less than 3 mg/cm^2, as shown in Figure S5a in the SI. Figure 2i shows the digital images of the free-standing binder-free Ni@NiO membrane annealed at 350 °C, which possesses high flexibility without any obvious mechanical damage even under severe bending conditions. Furthermore, we have measured the electrical conductivity of the membrane with different bending curvatures. The corresponding $I-V$ curves of the membrane without stress (black line) and with severe bending stress (red line) are shown in Figure S5b in the SI. In fact, over 100 bending cycles were taken before we obtained these $I-V$ curves. We found that all $I-V$ curves exhibited symmetrical linearity, which means that the metal wire and the sample have a very good ohmic contact. It can be clearly seen that the $I-V$ curve is very stable even with these intensive bending actions. It indicates that stresses do not have much obvious effect on the electrical conductivity of the membrane. Therefore, we have demonstrated that our membrane is tough and highly conductive, and these characteristics make it suitable for a practical flexible supercapacitor electrode. We believe this feature can be attributed to the robust mechanical bonding and strong weld among Ni@NiO nanowires.

The transmission electron microscopy (TEM) image of Ni@NiO nanowires in Figure 3a further confirms the result shown in SEM images, revealing that the nanowire is composed of a lot of Ni nanoparticles aligned by a magnetic field because of their magnetic anisotropy.[39] In addition, Figure 3b shows the high-resolution transmission electron microscopy (HRTEM) image of the surface of one nanowire. The Ni and NiO phase can be identified according to the lattice spacings, where 0.240 nm corresponds to the spacing of (111) planes of NiO and 0.203 nm corresponds to the spacing of {111} planes of Ni. Figure 3c shows a high angle annular dark field (HAADF) scanning TEM image of two Ni@NiO nanowires. Parts d and e of Figure 3 show energy-dispersive X-ray spectrometry (EDS) elemental mapping scan results of the nanowires taken from the framed region of Figure 3c for elements Ni and O, respectively. In particular, Figure 3e shows a clear NiO shell structure giving the distribution of the O element. The mapping result is

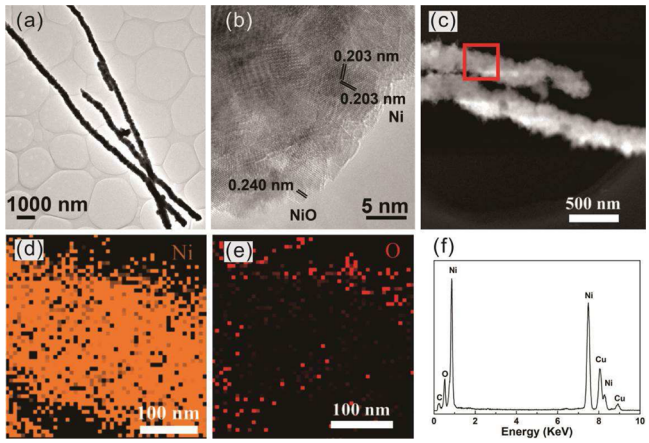

Figure 3. (a) TEM image of three Ni@NiO nanowires. (b) HRTEM image of the surface of one nanowire, indicating the polycrystalline characteristic. (c) HAADF scanning TEM image of two Ni@NiO nanowires. EDS elemental mapping scan results of the nanowires taken from the framed region of part c for elements (d) Ni and (e) O, respectively. (f) EDS of Ni@NiO nanowires.

consistent with the EDS spectrum shown in Figure 3f, in which traces of the C and Cu elements come from C membrane and Cu grid, respectively. Therefore, we believe that this microscopic evidence could demonstrate the Ni core/NiO shell nanowire structure more than enough. More detailed EDS spectral data are shown in Figure S6 in the SI taken from a larger area in SEM, indicating the increasing content of NiO with increasing annealing temperature.

Figure 4a shows cyclic voltammetry (CV) curves of a Ni@NiO membrane supercapacitor electrode with different annealing temperatures at a scan rate of 50 mV/s in a 1 M KOH aqueous solution (using a standard three-electrode system). The shapes of the CV curves are nearly symmetrical with two peaks of the redox currents, which is different from those of EDLCs with rectangular CV curves. The redox peaks of NiO are caused by the faradaic oxidation/reduction reactions as follows:[40]

$$\mathrm{NiO} + \mathrm{OH}^- \leftrightarrow \mathrm{NiOOH} + \mathrm{e}^- \quad (1)$$

The three CV curves were similar in shape, indicating the same NiO faradaic reactions. Furthermore, the binder-free electrode oxidized at 350 °C shows a significantly better performance than its high-temperature counterparts. The galvanostatic charge/discharge measurements (at the current density of 0.064 A/cm^3) also show the same situation, as shown in Figure 4b. There are two reasons for the better performance of the sample calcined at 350 °C. On the one hand, a rough and echinate surface (as shown in the SEM images) could provide more interface area between the active NiO layer and electrolyte, ensuring efficient diffusion paths for the OH^- ions. Therefore, such a structure can significantly accelerate intercalation of the electrolyte ions and improve utilization of the active electrode material.[41] On the other hand, the conductive network of Ni nanowire cores is well-preserved when the annealing temperature stays relatively low (350 °C). Higher annealing temperature could increase the thickness of the NiO layer, which results in isolation of the conductive Ni nanowire cores and a much poorer conductivity. This situation is consistent with the changing trend of the sheet resistance for the three samples. Poorer conductivity could hinder the efficient utilization of the active electrode material in turn,

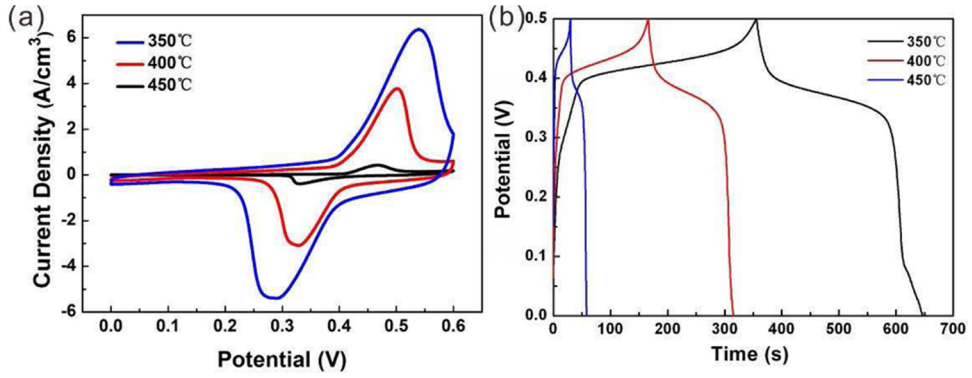

Figure 4. (a) CV curves at a scan rate of 50 mV/s. (b) Galvanostatic charge/discharge behavior (at a current density of 0.064 A/cm^3) of Ni@NiO nanowire membrane electrodes with different annealing temperatures in a 1 M KOH aqueous solution.

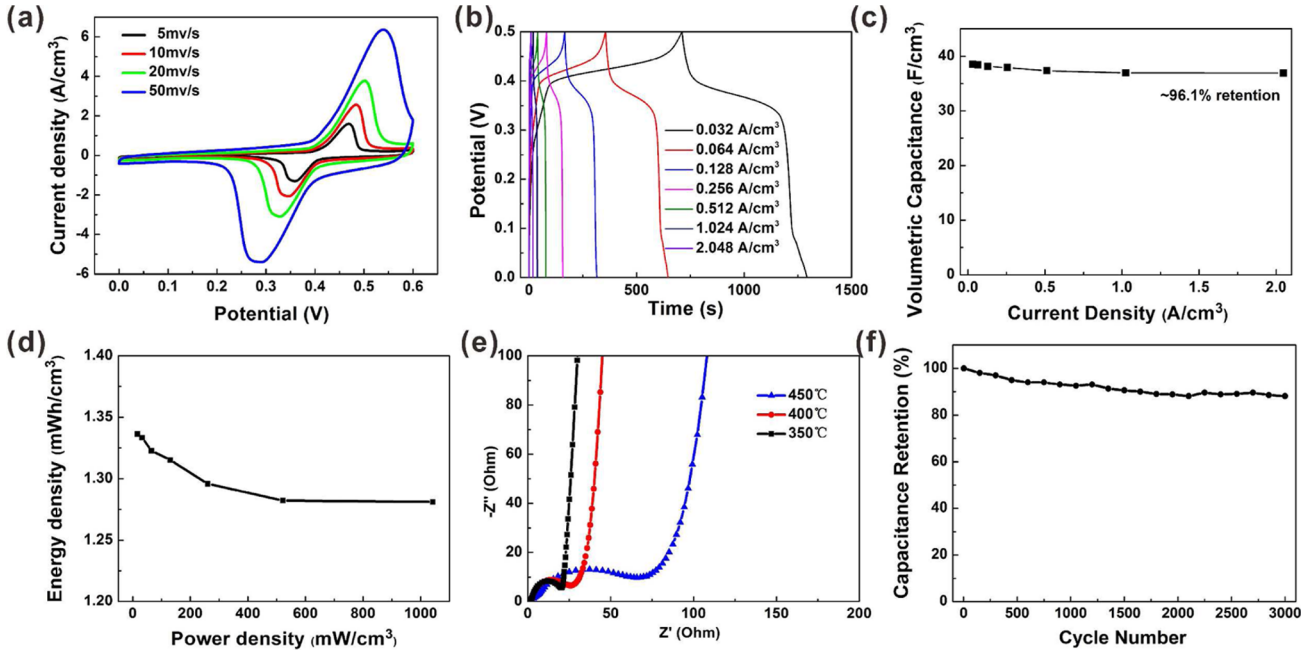

Figure 5. (a) CV curves of the sample with an annealing temperature of 350 °C at different scan rates ranging from 5 to 50 mV/s. (b) Galvanostatic charge/discharge behavior of the sample with current densities of up to 2.048 A/cm^3. (c) Volume capacitance with respect to the current density. (d) Ragone plot. (e) Nyquist plot of supercapacitor electrodes with different annealing temperatures. (f) Curve of the cycle life test at a current density of 0.512 A/cm^3.

owing to polarization loss.[42,43] This reason can be further supported by the electrochemical impedance spectroscopy (EIS) data shown in Figure 5e. Experimental results show that solution resistance (R_S, referring to the resistance from the electrolyte[37]) is insensitive to the surface condition of the electrode, and it is consistent with a value of around 1.4 Ω for all of our samples. The charge-transfer resistance (R_{CT}, or Faraday resistance, corresponding to the total resistance at the interface between the electrode and electrolyte[37]) of the sample with annealing temperatures from over 350 °C, through 400 °C, to 450 °C increases from about 18 Ω, through 24 Ω, to 66 Ω. This implies that a thick NiO layer would increase R_{CT} and hinder the transfer of electrons produced by faradaic reaction between NiO and OH^-. Meanwhile, the slope of the sample at lower frequencies with 350 °C annealing temperature is much bigger than that of the sample with higher temperature, indicating better capacitive behavior.[17]

Because the binder-free electrode annealing at 350 °C has the best supercapacitor performance, more detailed characterizations have been performed based on this sample. Figure 5a shows CV curves of the sample at different scan rates ranging from 5 to 50 mV/s. All CV curves (Figure 5a) exhibit similar shape, and the peak current increases with rising scan rates. The shape of the CV curve does not transform very much even at a high scan rate of 50 mV/s, revealing the good kinetic reversibility of the binder-free Ni@NiO electrodes. Especially, the peak potential shifts only about 50 mV for a 10 times increase in the scan rate owing to low polarization of the 3D nanostructured electrode.[44,45] In order to demonstrate the flexibility of our supercapacitor electrode, CV tests at different bending states were conducted. As shown in Figure S7 in the SI, the curvature only has a small influence on the electrochemical performance. The most important advantage of supercapacitors toward ordinary batteries is their much higher power density. Therefore, the high-power performance of the electrodes was characterized by a series of galvanostatic charge/discharge measurements with charge/discharge current densities of up to 2.048 A/cm^3 (Figure 5b). Obviously, the

nonlinearity in the charge/discharge curves further confirms the pseudocapacitance behavior of NiO originating from the Faraday reaction.[15] The volumetric capacitances with respect to the current densities are derived from galvanostatic charge/discharge curves and plotted in Figure 5c. Here we use volumetric capacitance as a standard for characterization (by using the overall volume of the supercapacitor electrode).[46] For a more comprehensive characterization, we also calculated the specific capacitance (by using the mass loading of active NiO), as shown in Figure S8 in the SI. The mass loading of active materials (NiO) for our sample is about 72.5 mg/cm^3. The value of capacitance is calculated following other literature reported.[37] The specific capacitance turns out to be about 530 F/g at a current density of 0.032 A/cm^3 and retains 510 F/g at a current density of 2.048 A/cm^3. The reversible redox reaction between NiO and OH^- (eq 1) is a highly diffusion-controlled process.[47] As a consequence, capacitance, and thus the obtained energy density, will suffer from a significant reduction at high charge/discharge rate. This familiar phenomenon has been observed in most of the previous studies.[15,18,37,44] While for our sample, the corresponding volumetric capacitance also tends to decrease with increasing current density, with an increase in the current density from 0.032 to 2.048 A/cm^3 by about 64 times, the supercapacitor electrode still preserves capacitance retention of about 96.1%, which indicates its wonderful rate capability. Compared with other pseudocapacitors, maybe the volumetric capacitance value of our sample is moderate, but the capacitance retention at high rate is undoubtedly remarkable. As the current density increases, the capacitance value at 2.048 A/cm^3 (about 36.9 F/cm^3) shows only a ~4% loss toward that obtained at a current density of 0.032 A/cm^3 (38.4 F/cm^3). The volumetric energy and power density of the overall electrode are two other crucial parameters for practical applications. According to the Ragone plot (Figure 5d), the highest energy density is about 1.34 mW·h/cm^3 with a power density of about 16.3 mW/cm^3 and still remains above 1.28 mW·h/cm^3 at 1.04 W/cm^3. These values are comparable with other binder-free electrodes or graphene oxide and onionlike carbon-based microsupercapacitor electrodes.[21,29,32,48,49] Particularly, such a high retention of energy density at high rate is very rare for pseudocapacitors and also splendid for EDLCs.[15,18,37,48,49] Cycling stability is another crucial issue for the supercapacitor electrode performance. Therefore, cycling tests were carried out using a high current density of 0.512 A/cm^3, as shown in Figure 5f. After 3000 charge/discharge cycles even at high rate, the capacitance retention is still about 89% (competitive with most works reported in the literature for analogous electrode systems[40,44]), implying that the sample has good electrochemical stability. Furthermore, the 3000 charge/discharge cycles did not degrade the flexibility and mechanical performance of the electrode, which is very important for practical application. Also, the Nyquist plots for 0 cycles and after 3000 cycles almost overlap (Figure S9 in the SI), indicating perfect stability of the electrode materials and good reversibility of the redox, which is consistent with the results of the cycle life test. Compared with common substrates, the binder-free Ni@NiO electrode shows great advantages in weight and thickness (2.93 mg/cm^2 in weight and a thickness of 26 μm). Especially, it is even lighter than ordinary A4 paper by two times and conforms to the description of "as light as a feather". This feature could meet the requirements of portable electronic products that have grown quickly in the past decade.

Essentially, the significant improvement of the capacitive performance at high rate for our sample can be attributed to synergistic effects of 3D Ni@NiO core−shell nanowire networks. When the NiO layer has an appropriate thickness, efficient current collection and unobstructed electron transport can be ensured by the well-preserved conductive network, which is composed of highly conductive core Ni nanowires welded and embeded to each other. Because the active NiO layer was formed by direct oxidation on the surface of a Ni nanowire, good electrical contact between the Ni core and NiO shell can be guaranteed, which is very useful for a fast faradaic redox. The unique 3D mesporous structure and nanoscale thorns on the surface of the nanowires can accelerate the intercalation and deintercalation velocity of electrolyte ions into the active materials. Meanwhile, this multigrade mesporous structure also can provide numerous electroactive sites for the Faraday reaction. Also, the whole 3D binder-free electrode playing the role of "ion-buffering reservoir" could assist a quicker permeation process of the electrolyte into each electroactive site by shortening the diffusion distances of OH^- and releases the strain originating from high rate insertion and extraction of OH^- ions.[45] As a result, a large number of electroactive sites can still be preserved at high rate, leading to a remarkable high rate capability.

CONCLUSION

In summary, an ultrathin and lightweight free-standing binder-free 3D Ni@NiO nanowire membrane was fabricated by a simple solution method under a 0.2 T magnetic field and a subsequent process including filtration together with thermal annealing. With an appropriate annealing temperature (350 °C), the surface of the Ni@NiO core−shell nanowires can still keep their rough and echinate surface, and the conductive network of Ni nanowire cores is well-preserved without isolation (0.53 Ω/sq in sheet resistance). Meanwhile, the unique 3D multigrade mesporous structure not only accelerates the intercalation and deintercalation velocity of electrolyte ions into the active NiO layer but also provides numerous electroactive sites for the Faraday reaction. Therefore, owing to these advantages, this supercapacitor electrode can still preserve a capacitance retention of about 96.1% (about 36.9 F/cm^3 at a current density of 2.048 A/cm^3) even with an increase of the current density by about 64 times, showing its wonderful rate capability. The fabricated supercapacitor electrode exhibits high volumetric capacitance, stable cycling life, remarkable retention of capacitance at high rate, and high energy and power density, making it a promising candidate for application in portable electronic products.

EXPERIMENTAL SECTION

Fabrication of a Free-Standing Ni@NiO Membrane Electrode. Ultralong Ni nanowires were synthesized by a simple liquid-phase method reported previously.[39] We took this method with a slight modification. In brief, 50 mL of 0.1 M $NiCl_2·6H_2O$, 200 mL of 1.5 M NaOH, and 150 mL of an ethylene glycol (EG) solution of $N_2H_4·H_2O$ (100 mL, 85 wt %) were mixed together in a flask. Then, 2 wt % poly(vinylpyrrolidone) (PVP) was added to the mixture. The mixture reacted at 70 °C for 1 h with the help of an applied 0.2 T magnetic field (as shown in Figure S1 in the SI). A Ni nanowire membrane was obtained after the products were cleaned, vacuum dried, redispersed in a 1 wt % EG solution of PVP, suction-filtered, dried, and stripped. By changing the quality of the Ni nanowires, we can get membranes with different thicknesses. The prepared Ni nanowires were first pressed at 10 MPa and then preannealed in a

horizontal tube furnace at 300 °C for 1 h at an atmosphere of H_2/Ar (V_{H_2}:V_{Ar} = 10:90). To achieve the active material of NiO, the Ni nanowire membrane was then annealed in a muffle furnace at 350 °C (at 400 or 450 °C) for only 5 min in the open air. Finally, a free-standing binder-free Ni@NiO core−shell nanowire membrane can be achieved. For convenience of the follow-up characterization, all of the Ni@NiO membranes were cut into 1 × 1 cm.

Characterizations and Electrochemical Tests. TGA was performed with a heating rate of 10 °C/min in air on a thermal analyzer (Pyris1 TGA, PerkinElmer Instruments). The crystal structures, morphologies, microstructures, and elementary compositions of the products were characterized by XRD (PANalytical BV X'Pert PRO), field-emission SEM (FEI Nova Nano-SEM 450), TEM (FEI Titan G2 60-300), and EDS (Nova nanoSEM, FEI). Nitrogen adsorption/desorption isotherms were measured at liquid-nitrogen temperature using a Micromeritics Tristar 3000 analyzer. All of the electrochemical measurements were carried out in a three-electrode system with 1 M KOH as the electrolyte at room temperature using an Autolab PGSTAT302N (Metrohm AG). EIS was carried out at 10 mHz to 100 kHz.

■ ASSOCIATED CONTENT

Ⓢ Supporting Information

Schematic diagram of the preparation for ultralong Ni nanowires, SEM images of commercial Ni foam, TGA curve of a free-standing Ni nanowire membrane, enlarged SEM images of the ultrathin Ni@NiO nanowire membrane, weight of the Ni@NiO nanowire membrane electrode after 350 °C calcination, *I*−*V* curves of the membrane without bending and with severe bending, detailed EDS spectral data from a larger area in SEM from a 3D mesporous free-standing Ni@NiO nanowire membrane with different annealing conditions, CV of the membrane electrode at different bending states, specific capacitance data of the binder-free electrode at various current densities, and Nyquist plots of the membrane electrode before and after 3000 cycles. This material is available free of charge via the Internet at http://pubs.acs.org.

■ AUTHOR INFORMATION

Corresponding Authors

*E-mail: nishuang_liu@foxmail.com.
*E-mail: gaoyihua@hust.edu.cn.

Notes

The authors declare no competing financial interest.

■ ACKNOWLEDGMENTS

This work was supported by the National Basic Research Program of China (Grant 2011CB933300), the National Natural Science Foundation of China (Grants 11204093 and 11074082), and "the Fundamental Research Funds for the Central Universities" (HUST: Grants 2014TS124 and 2013TS033). Thanks to facility support of the CNCD, WNLO-HUST.

■ REFERENCES

(1) Winter, M.; Brodd, R. J. What are Batteries, Fuel Cells, and Supercapacitors? *Chem. Rev.* **2004**, *104*, 4245−4269.
(2) Zhang, L. L.; Zhao, X. S. Carbon-based Materials as Supercapacitor Electrodes. *Chem. Soc. Rev.* **2009**, *38*, 2520−2531.
(3) Arico, A. S.; Bruce, P.; Scrosati, B.; Tarascon, J. M.; Van Schalkwijk, W. Nanostructured Materials for Advanced Energy Conversion and Storage Devices. *Nat. Mater.* **2005**, *4*, 366−377.
(4) Simon, P.; Gogotsi, Y. Materials for Electrochemical Capacitors. *Nat. Mater.* **2008**, *7*, 845−854.
(5) Conway, B. E. *Electrochemical Supercapacitors, Scientific Fundamentals and Technological Applications*; Kluwer Academic/Plenum: New York, 1999; p 736.
(6) Burke, A. R&D Considerations for the Performance and Application of Electrochemical Capacitors. *Electrochim. Acta* **2007**, *53*, 1083−1091.
(7) Burke, A. Ultracapacitors: Why, How, and Where is the Technology. *J. Power Sources* **2000**, *91*, 37−50.
(8) Miller, J. R.; Simon, P. Materials Science—Electrochemical Capacitors for Energy Management. *Science* **2008**, *321*, 651−652.
(9) Chmiola, J.; Yushin, G.; Gogotsi, Y.; Portet, C.; Simon, P.; Taberna, P. L. Anomalous Increase in Carbon Capacitance at Pore Sizes Less Than 1 Nanometer. *Science* **2006**, *313*, 1760−1763.
(10) Cheng, Y.; Lu, S.; Zhang, H.; Varanasi, C. V.; Liu, J. Synergistic Effects from Graphene and Carbon Nanotubes Enable Flexible and Robust Electrodes for High-Performance Supercapacitors. *Nano Lett.* **2012**, *12*, 4206−4211.
(11) Zhu, Y.; Murali, S.; Stoller, M. D.; Ganesh, K. J.; Cai, W.; Ferreira, P. J.; Pirkle, A.; Wallace, R. M.; Cychosz, K. A.; Thommes, M.; Su, D.; Stach, E. A.; Ruoff, R. S. Carbon-Based Supercapacitors Produced by Activation of Graphene. *Science* **2011**, *332*, 1537−1541.
(12) Lang, X. Y.; Hirata, A.; Fujita, T.; Chen, M. W. Nanoporous Metal/Oxide Hybrid Electrodes for Electrochemical Supercapacitors. *Nat. Nanotechnol.* **2011**, *6*, 232−236.
(13) Brezesinski, T.; Wang, J.; Tolbert, S. H.; Dunn, B. Ordered Mesoporous Alpha-MoO_3 with iso-oriented Nanocrystalline Walls for Thin-film Pseudocapacitors. *Nat. Mater.* **2010**, *9*, 146−151.
(14) Liu, J. P.; Jiang, J.; Cheng, C. W.; Li, H. X.; Zhang, J. X.; Gong, H.; Fan, H. J. Co_3O_4 Nanowire@MnO_2 Ultrathin Nanosheet Core/Shell Arrays: A New Class of High-Performance Pseudocapacitive Materials. *Adv. Mater.* **2011**, *23*, 2076−2081.
(15) Lu, Q.; Lattanzi, M. W.; Chen, Y. P.; Kou, X. M.; Li, W. F.; Fan, X.; Unruh, K. M.; Chen, J. G. G.; Xiao, J. Q. Supercapacitor Electrodes with High-Energy and Power Densities Prepared from Monolithic NiO/Ni Nanocomposites. *Angew. Chem., Int. Ed.* **2011**, *50*, 6847−6850.
(16) Xia, X. H.; Tu, J. P.; Zhang, Y. Q.; Wang, X. L.; Gu, C. D.; Zhao, X. B.; Fan, H. J. High-Quality Metal Oxide Core/Shell Nanowire Arrays on Conductive Substrates for Electrochemical Energy Storage. *ACS Nano* **2012**, *6*, 5531−5538.
(17) Yu, G. H.; Hu, L. B.; Liu, N. A.; Wang, H. L.; Vosgueritchian, M.; Yang, Y.; Cui, Y.; Bao, Z. A. Enhancing the Supercapacitor Performance of Graphene/MnO_2 Nanostructured Electrodes by Conductive Wrapping. *Nano Lett.* **2011**, *11*, 4438−4442.
(18) Liu, N. S.; Ma, W. Z.; Tao, J. Y.; Zhang, X. H.; Su, J.; Li, L. Y.; Yang, C. X.; Gao, Y. H.; Golberg, D.; Bando, Y. Cable-Type Supercapacitors of Three-Dimensional Cotton Thread Based Multi-Grade Nanostructures for Wearable Energy Storage. *Adv. Mater.* **2013**, *25*, 4925−4931.
(19) Liang, Y. Y.; Schwab, M. G.; Zhi, L. J.; Mugnaioli, E.; Kolb, U.; Feng, X. L.; Mullen, K. Direct Access to Metal or Metal Oxide Nanocrystals Integrated with One-Dimensional Nanoporous Carbons for Electrochemical Energy Storage. *J. Am. Chem. Soc.* **2010**, *132*, 15030−15037.
(20) Zhu, T.; Chen, J. S.; Lou, X. W. Shape-controlled Synthesis of Porous Co_3O_4 Nanostructures for Application in Supercapacitors. *J. Mater. Chem.* **2010**, *20*, 7015−7020.
(21) Yuan, C.; Yang, L.; Hou, L.; Li, J.; Sun, Y.; Zhang, X.; Shen, L.; Lu, X.; Xiong, S.; Lou, X. W. Flexible Hybrid Paper Made of Monolayer Co_3O_4 Microsphere Arrays on rGO/CNTs and Their Application in Electrochemical Capacitors. *Adv. Funct. Mater.* **2012**, *22*, 2560−2566.
(22) Mukherjee, R.; Thomas, A. V.; Krishnamurthy, A.; Koratkar, N. Photothermally Reduced Graphene as High-Power Anodes for Lithium-Ion Batteries. *ACS Nano* **2012**, *6*, 7867−7878.
(23) Park, J. H.; Lee, T. W.; Kang, M. G. Growth, Detachment and Transfer of Highly-ordered TiO_2 Nanotube Arrays: Use in Dye-sensitized Solar Cells. *Chem. Commun.* **2008**, 2867−2869.

(24) Zhang, X. W.; Zhang, T.; Ng, J.; Sun, D. D. High-Performance Multifunctional TiO_2 Nanowire Ultrafiltration Membrane with a Hierarchical Layer Structure for Water Treatment. *Adv. Funct. Mater.* **2009**, *19*, 3731−3736.
(25) Yuan, J. K.; Liu, X. G.; Akbulut, O.; Hu, J. Q.; Suib, S. L.; Kong, J.; Stellacci, F. Superwetting Nanowire Membranes for Selective Absorption. *Nat. Nanotechnol.* **2008**, *3*, 332−336.
(26) Pushparaj, V. L.; Shaijumon, M. M.; Kumar, A.; Murugesan, S.; Ci, L.; Vajtai, R.; Linhardt, R. J.; Nalamasu, O.; Ajayan, P. M. Flexible Energy Storage Devices based on Nanocomposite Paper. *Proc. Natl. Acad. Sci. U. S. A.* **2007**, *104*, 13574−13577.
(27) Wang, R. H.; Xu, C. H.; Sun, J.; Liu, Y. Q.; Gao, L.; Lin, C. C. Free-standing and Binder-free Lithium-ion Electrodes based on Robust Layered Assembly of Graphene and Co_3O_4 Nanosheets. *Nanoscale* **2013**, *5*, 6960−6967.
(28) Niu, Z. Q.; Luan, P. S.; Shao, Q.; Dong, H. B.; Li, J. Z.; Chen, J.; Zhao, D.; Cai, L.; Zhou, W. Y.; Chen, X. D.; Xie, S. S. A "Skeleton/Skin" Strategy for Preparing Ultrathin Free-standing Single-walled Carbon Nanotube/Polyaniline Films for High Performance Supercapacitor Electrodes. *Energy Environ. Sci.* **2012**, *5*, 8726−8733.
(29) Perera, S. D.; Patel, B.; Nijem, N.; Roodenko, K.; Seitz, O.; Ferraris, J. P.; Chabal, Y. J.; Balkus, K. J. Vanadium Oxide Nanowire−Carbon Nanotube Binder-Free Flexible Electrodes for Supercapacitors. *Adv. Energy Mater.* **2011**, *1*, 936−945.
(30) Lu, X. J.; Dou, H.; Gao, B.; Yuan, C. Z.; Yang, S. D.; Hao, L.; Shen, L. F.; Zhang, X. G. A Flexible Graphene/Multiwalled Carbon Nanotube Film as a High Performance Electrode Material for Supercapacitors. *Electrochim. Acta* **2011**, *56*, 5115−5121.
(31) Wang, D. W.; Li, F.; Zhao, J. P.; Ren, W. C.; Chen, Z. G.; Tan, J.; Wu, Z. S.; Gentle, I.; Lu, G. Q.; Cheng, H. M. Fabrication of Graphene/Polyaniline Composite Paper via In Situ Anodic Electropolymerization for High-Performance Flexible Electrode. *ACS Nano* **2009**, *3*, 1745−1752.
(32) He, Y. M.; Chen, W. J.; Li, X. D.; Zhang, Z. X.; Fu, J. C.; Zhao, C. H.; Xie, E. Q. Freestanding Three-Dimensional Graphene/MnO_2 Composite Networks As Ultra light and Flexible Supercapacitor Electrodes. *ACS Nano* **2013**, *7*, 174−182.
(33) Rathmell, A. R.; Nguyen, M.; Chi, M.; Wiley, B. J. Synthesis of Oxidation-Resistant Cupronickel Nanowires for Transparent Conducting Nanowire Networks. *Nano Lett.* **2012**, *12*, 3193−3199.
(34) Kong, D. S.; Wang, J. M.; Shao, H. B.; Zhang, J. Q.; Cao, C. N. Electrochemical Fabrication of a Porous Nanostructured Nickel Hydroxide Film Electrode with Superior Pseudocapacitive Performance. *J. Alloys Compd.* **2011**, *509*, 5611−5616.
(35) Yuan, C. Z.; Li, J. Y.; Hou, L. R.; Zhang, X. G.; Shen, L. F.; Lou, X. W. Ultrathin Mesoporous $NiCo_2O_4$ Nanosheets Supported on Ni Foam as Advanced Electrodes for Supercapacitors. *Adv. Funct. Mater.* **2012**, *22*, 4592−4597.
(36) Grden, M.; Alsabet, M.; Jerkiewicz, G. Surface Science and Electrochemical Analysis of Nickel Foams. *ACS Appl. Mater. Interfaces* **2012**, *4*, 3012−3021.
(37) Chen, W.; Rakhi, R. B.; Hu, L. B.; Xie, X.; Cui, Y.; Alshareef, H. N. High-Performance Nanostructured Supercapacitors on a Sponge. *Nano Lett.* **2011**, *11*, 5165−5172.
(38) Zhang, J.; Fu, J.; Zhang, J.; Ma, H.; He, Y.; Li, F.; Xie, E.; Xue, D.; Zhang, H.; Peng, Y. Co@Co_3O_4 Core−Shell Three-Dimensional Nano-Network for High-Performance Electrochemical Energy Storage. *Small* **2014**, *10*, 2618−2624.
(39) Wang, J.; Wei, L. M.; Zhang, L. Y.; Jiang, C. H.; Kong, E. S. W.; Zhang, Y. F. Preparation of High Aspect Ratio Nickel Oxide Nanowires and Their Gas Sensing Devices with Fast Response and High Sensitivity. *J. Mater. Chem.* **2012**, *22*, 8327−8335.
(40) Kim, J. H.; Zhu, K.; Yan, Y. F.; Perkins, C. L.; Frank, A. J. Microstructure and Pseudocapacitive Properties of Electrodes Constructed of Oriented NiO−TiO_2 Nanotube Arrays. *Nano Lett.* **2010**, *10*, 4099−4104.
(41) Zheng, J. P.; Jow, T. R. A New Charge Storage Mechanism for Electrochemical Capacitors. *J. Electrochem. Soc.* **1995**, *142*, L6−L8.
(42) Weidner, J. W.; Timmerman, P. Effect of Proton Diffusion, Electron Conductivity, and Charge-Transfer Resistance on Nickel Hydroxide Discharge Curves. *J. Electrochem. Soc.* **1994**, *141*, 346−351.
(43) Lanzi, O.; Landau, U. Effect of Sinter Fracture and Ohmic Resistance on Capacity Retention in the Nickel Oxide Electrode. *J. Electrochem. Soc.* **1991**, *138*, 2527−2538.
(44) Liang, K.; Tang, X.; Hu, W. High-performance Three-dimensional Nanoporous NiO Film as a Supercapacitor Electrode. *J. Mater. Chem.* **2012**, *22*, 11062−11067.
(45) Lei, Y.; Li, J.; Wang, Y. Y.; Gu, L.; Chang, Y. F.; Yuan, H. Y.; Xiao, D. Rapid Microwave-Assisted Green Synthesis of 3D Hierarchical Flower-Shaped $NiCo_2O_4$ Microsphere for High-Performance Supercapacitor. *ACS Appl. Mater. Interfaces* **2014**, *6*, 1773−1780.
(46) Gogotsi, Y.; Simon, P. True Performance Metrics in Electrochemical Energy Storage. *Science* **2012**, *335*, 167−167.
(47) Yu, P. C.; Nazri, G.; Lampert, C. M. Spectroscopic and Electrochemical Studies of Electrochromic Hydrated Nickel Oxide Films. *Sol. Energy Mater.* **1987**, *16*, 1−17.
(48) Gao, W.; Singh, N.; Song, L.; Liu, Z.; Reddy, A. L. M.; Ci, L. J.; Vajtai, R.; Zhang, Q.; Wei, B. Q.; Ajayan, P. M. Direct Laser Writing of Micro-supercapacitors on Hydrated Graphite Oxide Films. *Nat. Nanotechnol.* **2011**, *6*, 496−500.
(49) Pech, D.; Brunet, M.; Durou, H.; Huang, P. H.; Mochalin, V.; Gogotsi, Y.; Taberna, P. L.; Simon, P. Ultrahigh-power Micrometre-sized Supercapacitors based on Onion-like Carbon. *Nat. Nanotechnol.* **2010**, *5*, 651−654.